# Remotely Monitored Buoys for Observing the Growth and Development of Sea Ice In Situ

RACHEL W. OBBARD, a,d ALICE C. BRADLEY, b,d AND IGNATIUS RIGORC

a SETI Institute, Mountain View, California
 b Geoscience Department, Williams College, Williamstown, Massachusetts
 c Polar Science Center, Applied Physics Laboratory, University of Washington, Seattle, Washington
 d Dartmouth College, Hanover, New Hampshire

(Manuscript received 4 November 2020, in final form 15 April 2022)

ABSTRACT: This paper describes a remotely monitored buoy that, when deployed in open water prior to freeze up, permits scientists to monitor not only temperature with depth, and hence freeze up and sea ice thickness, but also the progression of sea ice development}e.g., the extent of cover at a given depth as it grows (solid fraction), the brine volume of the ice, and the salinity of the water just below, which is driven by brine expulsion. Microstructure and In situ Salinity and Temperature (MIST) buoys use sensor "ladders" that, in our prototypes, extend to 88 cm below the surface. We collected hourly measurements of surface air temperature and water temperature and electrical impedance every 3 cm to track the seasonal progression of sea ice growth in Elson Lagoon (Utqiagvik, Alaska) over the 2017/18 ice growth season. The MIST buoy has the potential to collect detailed sea ice microstructural information over time and help scientists monitor all parts of the growth/melt cycle, including not only the freezing process but the effects of meteorological changes, changing snow cover, the interaction of meltwater, and drainage.

SIGNIFICANCE STATEMENT: There is a need to better understand how an increasing influx of freshwater, one part of a changing Arctic climate, will affect the development of sea ice. Current instruments can provide information on the growth rate, extent, and thickness of sea ice, but not direct observations of the structure of the ice during freeze up, something that is tied to salinity and local air and water temperature. A first deployment in Elson Lagoon in Utqiagvik, Alaska, showed promising results; we observed fluctuations in ice temperatures in response to brief warmings in air temperature that resulted in changes in the conductivity, liquid fraction, and brine volume fraction within the ice.

KEYWORDS: Arctic; Sea ice; Buoy observations; In situ oceanic observations

## 1. Introduction

Arctic sea ice has been declining in extent and thickness for as long as we have been remotely monitoring it (Comiso et al. 2008; IPCC 2014). Between 1979 and 2013, the Arctic melt season lengthened by approximately 5 days decade<sup>21</sup> due to later freeze up and earlier onset of melt (Stroeve et al. 2014). In 2012 there was a record minimum in summer sea ice extent and in 2018 the maximum (winter) sea ice extent hit a new low (Parkinson and Comiso 2013; NSIDC 2018; www.neptune.gsfc.nasa.gov).

The onset of freeze up in the Arctic as a whole was delayed by about 3 days over the period 2000–12 compared to 1982–99 (Steele et al. 2019). This effect, attributed to higher summer sea surface temperature (SST) and warmer September air temperatures, was most pronounced in the Arctic Basin. This and large discrepancies between predicted and actual freeze-up dates in some regions suggest a need to better understand the processes affecting freeze up on a regional scale (Stroeve et al. 2014).

Climate model simulations predict that a global temperature increase of over 48C by 2100 AD (RCP scenario 8.5; Collins et al. 2013) would also be accompanied by more precipitation

Corresponding author: Rachel W. Obbard, robbard@seti.org

over the North Atlantic (Bintanja and Andry 2017) and higher riverine input to the Arctic (Lehner et al. 2012; Nummelin et al. 2016). This will affect the timing and extent of sea ice (Bauch et al. 2013; Nghiem et al. 2014).

To better observe and understand both the physical processes and growth rate of landfast sea ice, and ultimately the effect of increased freshwater on sea ice development, we developed an instrumented buoy to monitor the structural development of sea ice (Nghiem et al. 2014; Nummelin et al. 2016). Satellite data can provide information on growth rate, extent, and thickness, but not direct observations of the physical processes of freeze up. Insight into these processes is important because they affect the microstructure of the ice (Nakawo and Sinha 1984; Light et al. 2003; Petrich et al. 2006; Notz and Worster 2008). Microstructure in turn affects its optical properties (e.g., albedo and transmissivity), thermodynamic properties (thermal conductivity and heat capacity), thickness, porosity (total and effective), permeability, fluid transport, and electrical properties (Grenfell 1983; Eicken 2000; Light et al. 2004; Carpenter et al. 2005; Petrich et al. 2006; Worster and Rees Jones 2015).

Most microstructural observations of sea ice have been made in laboratory settings (e.g., Golden et al. 2007), or at discrete depth intervals, using samples removed from the ice cover (Obbard et al. 2009, 2016; Lieb-Lappen et al. 2017a,b). The development described herein was in part an effort to

DOI: 10.1175/JTECH-D-20-0183.1

study microstructural and microchemical development in the natural environment and driven by our previous work done to understand the evolution and topology of brine networks (Lieb-Lappen et al. 2017a,b). Our buoy is based on a technique and instrumentation known as the "wire harp," developed by Notz et al. (2005). It contains two extended wire harps (herein called wire ladders), that measure sea ice and water properties to 88 cm depth. The wire ladder, consisting of pairs of conductive wires parallel to and at increasing distance from the surface, is suspended in the water column. As ice grows downward around the instrument, electrical impedance between the wire pairs changes with bulk salinity and can be used to derive solid fraction. This process is described in more detail in section 2c.

Previously, wire harps have been deployed by cutting a large (21 m square) hole in existing sea ice cover, suspending the wire harp in the seawater that floods the open hole, and allowing the ice to refreeze over a period of days to a week (Notz et al. 2005; Notz and Worster 2008). Data are recorded on an SD card in a weatherproof box resting on the ice nearby and is collected by visiting the site and downloading the data from the SD card. The instrument is then retrieved by cutting the block of newly formed ice containing it from the surrounding ice. We deployed a wire harp in this manner in 2015 and found that because the new ice forms not only from the surface down, but also from the sides of the hole in, the sea ice ocean interface around the wire harp is hemispherical and the data collected using this method are not 100% representative of the growth process and structure of newly formed sea ice in the open ocean. The solution is to deploy the wire harp in open water before freeze up, but this requires a buoy that can survive the dynamic forces of freeze up. During the consolidation process, pancake ice bashes equipment and thin ice is particularly prone to deformation during rafting and ridging.

The Microstructure and In situ Salinity and Temperature (MIST) buoy includes a robust frame that protects two extended (21 m) wire ladders from the dynamic damage of the initial stages of freezing sea ice while allowing the ice to grow down around the wires in as close to a natural growth pattern as possible. A supporting electronics package logs data, and radios data (including location, in case the buoys drift) to the researchers throughout the winter so that repeated site visits are not required.

Two of these buoys were deployed over winter of 2017/18 in Elson Lagoon, near Utqiagvik, Alaska. They survived potentially damaging conditions with little structural harm to the instruments, and logged measurements of ice temperature and conductivity through the winter (Bradley et al. 2020).

## 2. Background

# a. Observing the sea ice development process

There have been a number of instruments developed to monitor seasonal changes in sea ice thickness and the International Arctic Buoy Program (IABP) has maintained an autonomous observing network since 1979, with buoys deployed initially on multiyear ice flows by ships and aircraft,

and later in open water during summer in response to the increasing area of the dynamic seasonal ice zone (Strong and Rigor 2013).

The autonomous ice mass-balance buoy (IMB), deployed since 2000, collects data on snow accumulation and ablation, ice growth and melt, and internal ice temperature, which can determine whether changes in ice-cover thickness occur at the top or bottom. This helps scientists understand the driving force behind changes.

The IABP has also been deploying Surface Velocity Program (SVP) Lagrangian drifting buoys (e.g., Centurioni et al. 2017), and has developed the Seasonal Ice Beacon (XIB), which is designed to survive in the seasonal ice zone (Comiso et al. 2019). Other, lower cost, autonomous instrumentation has also been developed that makes it possible to measure a temperature profile in the ice and even resolve material interfaces to within a few centimeters (Jackson et al. 2013).

While there are a number of instruments to measure the evolution of sea ice thickness, and the basics of columnar sea ice growth are well understood, it is difficult to observe the development of the sea ice microstructure in situ. This is in large part due to the difficulty in placing sensors in the ice early in the winter growth season. Wire harp sensors, described in more detail below, have been temporarily installed in artificial leads several months into the growth season, when travel on sea ice is safe (Notz et al. 2005; Notz and Worster 2008).

All such buoys face challenges in protecting the instruments from snow, wind, wildlife, and low temperatures over long periods, and we built on this expertise to develop the MIST buoys.

# b. How the wire harp works

Notz's "wire harp" instrument is based on the principle that pure solid ice is a good electrical insulator whereas interstitial saltwater brine is a good conductor (Notz et al. 2005; Notz and Worster 2008). The device records temperature and resistivity at different depths as ice grows around it. Salinity of the interstitial brine is then inferred from the liquidus relationship (Cox and Weeks 1986) and can be combined with the measured solid mass fraction to give the bulk salinity profile of the growing sea ice. The wire harp is a set of modules, each holding eight pairs of 0.25-mm-diameter wires. One end of each pair is set in epoxy resin, and the other end is attached to a narrow strip of polycarbonate for stability. Each wire in a pair is separated by 5 mm from its mate, and the pairs are evenly spaced 5-25 mm apart vertically. The base of each module is fastened to a post so that the wire pairs lie horizon-tal in the water, one beneath another, in an "artificial lead" or hole cut in existing sea ice. The vertical height of the whole apparatus (and ice thickness that can be measured), as well as the depth resolution, depends on the number of modules and wire pair spacing. The temporal resolution is fractions of a second. The associated electronics package, which consists of a signal generator, amplifier, and datalogger, is housed in a waterproof box at the surface and runs off a battery. By measuring the electrical impedance between the two wires of each

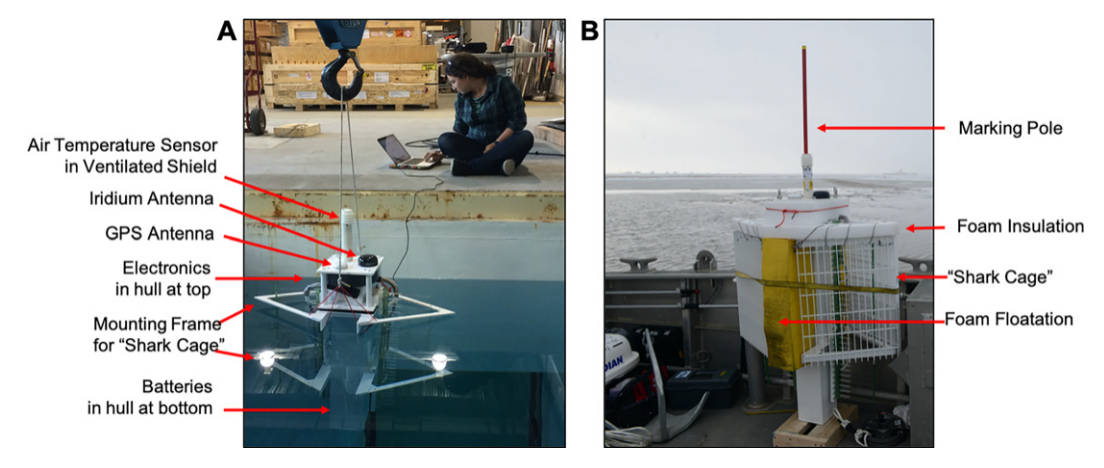


Fig. 1. MIST buoy and its components. (a) Open (without protective and floatation components) in the test pool at the University of Washington; (b) the fully assembled Eyak MIST buoy ready for deployment.

pair, it is possible to calculate the average solid volume fraction of the sea ice forming along the wires, from which the solid mass fraction can be derived.

Thermistors are mounted on the instrument at the levels of the wire pairs to measure the temperature (T) in the ice at that depth. The liquid fraction  $(1\ 2\ F)$  at a given depth is a function of the ratio of the impedance  $Z_0$  when ice starts to form and the impedance at a lower temperature Z, and the change of the conductivity g of the interstitial brine with salt concentration and temperature (Notz et al. 2005):

1 2 F 
$$\frac{g}{g(T, S)} \frac{Z_0}{Z}$$
,

where S is the brine concentration at the depth of the wire pair as calculated from the liquidus relationship for seawater [POLY3 computation method from Vancoppenolle et al. (2019)]. It can be expressed as

$$S = 20:00535T^3 = 20:519T^2 = 218:7T$$

where  $Z_0$  is found by identifying the time when ice formed around the wires, and then set the reading just before then to  $Z_0$ . This can be done by eye or with an algorithm. The algorithm first isolates the readings when temperature is close to freezing, and then searches for the beginning of a monotonic increase.

The derivation of expressions for the conductivity of the brine when the ice starts to form  $(g_0)$  and of the interstitial brine (g) are found in Notz et al. (2005).

# 3. Materials and methods

#### a. MIST buoy design

When deployed, the MIST buoys (Fig. 1) recorded location, air temperature, and sets of paired temperature and electrical impedance measurements below the water level. The buoys included measurement and communications subsystems and a control subsystem housed in a ruggedized

structure. These components are described in the sections that follow.

#### 1) Measurements subsystem

Fundamental to the MIST buoy are the wire harps and their control hardware, which were developed and manufactured by Dirk Notz's group at the Max-Planck-Institut für Meteorologie. Each MIST buoy has two wire ladders. Each ladder is made of four separate wire harp modules and each module has, at 3 cm intervals, eight pairs of horizontal wires and a temperature sensor. The four modules on either side of the buoy extend 93 cm, from the top wire pair to the bottom. They are attached to the buoy such that the float line falls between the second and third wire, and the top two are above freeboard, and can measure approximately 88 cm of ice growth. The wires are 14 cm long, with a 4 cm insulated buffer at the inside end to shield the measurements from the influence of the main body of the buoy.

Each buoy also contains other measurement devices, controlled by a central datalogger (Campbell Scientific C300). Location is tracked with a Garmin 16X GPS. The patch antenna is affixed to the top platform of the buoy, to keep it as close to above the snow level as possible. It typically took about 45 s to get a position solution. Over the course of the winter season deployment, it seemed to be accurate to 10-15 m, even with the antenna covered in a few inches of snow. An air temperature sensor (Campbell Scientific 109LL) was mounted on a post above the top platform, which kept it above the snow level in all but the most ex-treme drifting circumstances. An X-Y tiltmeter (Campbell Scientific CXTA02-T) was used to monitor the angle of the buoy relative to a perfectly vertical float. If a buoy tilted, the wire pairs would be at an angle relative to the water surface and could measure ice characteristics at different depths than those measured by the temperature sensors, and with the wires 14 cm in length, the depths measured by different wires could overlap. These measurements were only used as quality assurance.

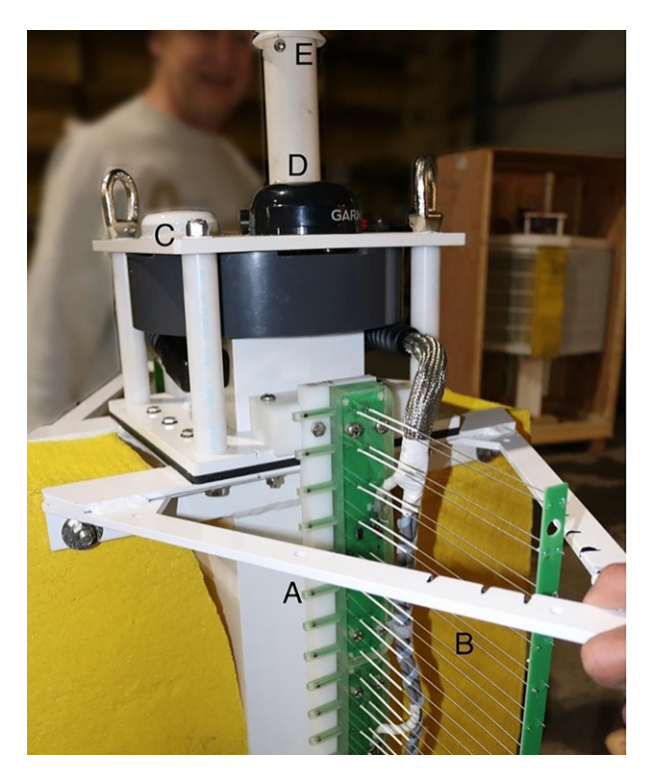


FIG. 2. MIST buoy without the protective cages, showing the wire harp sensors: (a) temperature sensors, (b) wire pairs, (c) Iridium SBD antenna, (d) GPS unit, and (e) air temperature sensor.

Basic operation consisted of a control subsystem that directed a datalogger to collect one set of observations including air temperature, tilt, GPS position, and the full set of harp measurements per hour, store it locally, package that hours' data, and transmit the data via Iridium short burst data (SBD).

# 2) CONTROL SUBSYSTEM

The control board operated the modules, sending out a pulse of alternating current to each wire pair in succession and logging each electrical impedance measurement from between the wires (as shown in Fig. 2).

A Campbell Scientific C300 datalogger managed the measurement process. Once per hour, the C300 woke from sleep mode. The GPS was powered on, recorded the latitude and longitude of the buoy and the current time, and sent these data to the C300. The GPS time was used in the recorded time stamp, instead of relying on the internal datalogger clock. Following location acquisition, the GPS was powered down and the multiplexer switched the serial connection to connect to the wire ladders. The datalogger then sampled and recorded the air temperature, averaged over 10 s, and the X–Y tilt (instantaneous). The wire ladders were powered on and allowed to collect data for several minutes. Once a full data acquisition cycle was complete, the wire ladders were powered down and the Iridium modem powered on. The C300 datalogger packaged the most recent observations into a

data packet and transmitted the packet before powering down the Iridium modem and going into sleep mode. All observations were saved to the C300 datalogger internal memory in addition to being transmitted over the Iridium SBD network. Each sampling cycle took between 6 and 9 min.

The low-power (and relatively low cost) Campbell Scientific C300 datalogger has only one pair of serial Tx/Rx pins. This connection was needed both to receive data from the wire ladder control board, the GPS unit, and to send data to the Iridium modem. The GPS and wire ladder control subsystems were connected to the serial pins via a multiplexer chip switched using a digital control pin from the C300, and the Iridium used the built in RS-232 serial connection. To make this work, the GPS was powered on, position lock achieved, and the GPS data were received and stored before the GPS was powered down and the wire ladder control board turned on. At no point were the GPS and wire ladder control board operating at the same time. Thus, the stored position was several minutes old by the time the data were sent. However, the difference between stored position and actual position would have been small for Eyak, due to its drag anchor (described below).

#### 3) COMMUNICATIONS SUBSYSTEM

Rather than wait for buoy retrieval (in case something happened over the course of the winter and the buoy was lost), the data could be sent back in real time. An Iridium SBD modem relayed data back to the investigators throughout the season. Data packets were assembled by the C300 datalogger and sent hourly, when the Iridium modem was powered on for transmission. To conserve power, the Iridium modem was only used to send data from the buoy. If an hourly packet was missed, there was no way to request that it be resent: to get that hours' observations, the buoy must be recovered.

# 4) Buoy structure

The buoy structure (Fig. 1) was designed to protect fragile instruments from the potentially damaging forces associated with pancake ice and ice ridging. The buoy body consisted of a square aluminum column with space for the support electronics inside. The battery was mounted at the bottom to facilitate buoyant equilibrium, while the rest of the electronics were suspended from a frame that can be lifted out of the top of the buoy for easy assembly and to protect expensive components in case of a minor leak. This frame included portholes that lead to the GPS antenna, the Iridium antenna, and the air temperature sensor on the top plate of the buoy. The whole system was connected such that the top frame was a structurally sound lift point for the buoy, important for deployment and retrieval.

The antennas and temperature sensor were mounted to the top of a raised platform above the top frame of the buoy. This was lifted 15 cm above the top frame (20 cm above the designed float level) in order to keep these components above most of the snow and potential flooding. The air temperature sensor was mounted in a solar radiation shield an additional 15 cm above the platform. The limited lift height of the top

platform was a compromise between getting the antennas above the snow level and keeping the buoy structurally robust in case of getting run over by an ice floe during an ice deformation event.

The wire ladder modules were then mounted to the outside of the main body of the buoy, separated by 3 cm to a polycarbonate mounting plate and then an additional 2.5 cm to the temperature sensors on the modules. The wire pairs extended out perpendicular to the buoy body at that same distance and extended 14 cm to the end caps.

The instrument modules were then surrounded by the "shark cage," a frame of aluminum stair grating that protected the top meter of the buoy depth from collisions with pancake ice or compressional forces associated with ice deformation. The whole buoy was painted white to protect the metal and limit potential solar heating.

The buoy frame and the shark cage were topped with an 8-cm-thick layer of white closed cell foam. This was intended to limit heat transport through the buoy frame and shark cage rather than through the ice.

Finally, a reflective safety pole was attached to the top of the buoy to make it visible to passing snow machines. The two buoys were deployed in places that were not entirely out of the way of snow machine traffic out of Utqiagvik and needed to be visible to prevent people from crashing into a partially snow-covered top platform on the buoy.

The buoys were also outfitted with a hanging weight to maintain buoyant stability. For the buoy called Eyak, the first launched, a drag anchor made from a canvas sack of locally sourced sand and gravel was affixed with a 5 m rope to the same point on the buoy as the hanging weight in order to keep the buoy from drifting before sea ice froze up around it.

# b. Instrument accuracy

The two fundamental measurements collected by the wire harps are impedance and temperature. In laboratory testing, the temperature sensors had an absolute accuracy (after a single-point calibration) of 0.28C (around freezing point) to 0.58C (around 1128 and 2178C). In overnight open air tests before deployment, there was 0.28C variability in measured temperatures between the different sensors in the range of 278 to 2108C.

The instrument uncertainty in the impedance measurement is very small (1/10 000 of the measurement), but the uncertainty in the actual geometry of what is being measured (exactly the spacing, and any possible bends in the wires) is more sizable. This is why the analysis uses ratios of the measured impedance during the season to the initial impedance (when it was in mostly unfrozen water) instead of the measured values themselves. This assumes of course that the wire geometry does not change over time, which it should not unless it is subject to deformation as some of the wires at the very bottom were.

The bulk salinity values are based on the salinity profile measured with the SonTek Castaway CTD, which has an accuracy of 60.1 psu, just prior to buoy deployment. This was not exactly coincident with the timing of the first impedance

measurements, but we did compare initial salinity values measured by the buoy to the Sontek values and they were within 2 psu. The other calculated properties use the impedance ra-tio and temperature as described in Notz et al. (2005) and not the reference to the initial salinity.

#### c. Calibration

Prior to installation on the buoy, the temperature sensors on the wire ladders were calibrated using a single point calibration at 08C. Sensors were submerged in a cold-water bath (freshwater containing a large amount of freshwater ice) for 30 min in order for all channels to collect a temperature measurement several times. Bias correction terms for each sensor channel were calculated from these measurements. Most were biased slightly high, measuring 0.28–0.38C. These correction offsets were then applied to all measured data for each channel.

Once the buoys were fully assembled and ready to deploy, an overnight measurement collection was run to check the correction factors. The buoys sat outside on the snow-covered ground in an air temperature of approximately 2108 to 278C. In a sheltered area, surrounded by equipment and snow berms, there was no notable vertical temperature gradient, and the two buoys, with two vertical sensor ladders each, measured the same air temperatures over the course of the night. At these temperatures there was up to 0.28C variability between channels.

The conductivity measurement, being made by pairs of wires that were prone to bending or slight deformation, could not be accurately calibrated before deployment. Instead, salinity is calculated from the ratio of the measured impedance between two wires to the mean impedance between those same wires over the first six hours following deployment. The salinity calculation is then calibrated against the in situ salinity at the time of deployment, as measured with a SonTek Castaway CTD over the edge of the deployment vessel.

#### d. Deployment

In October 2017, two MIST buoys were deployed in Elson Lagoon (shown in Fig. 4), a shallow estuarine lagoon near Utqiagvik. This site was chosen because of its relatively protected nature as compared to open ocean locations in this region. Elson Lagoon is open to the Beaufort Sea in the north. In summer months it receives submarine groundwater discharge with contributions from fresh groundwater and water released from permafrost degradation (Dimova et al. 2015). Average water depth is only 2.4 m, and in the winter the sea ice freezes to the bottom of the lagoon (Harris et al. 2017) in places.

Due to shipping delays and a spell of cold weather, deployment took place during freeze up on the lagoon, which significantly hampered the process and resulted in several more days delay while accessible locations were scouted.

The first buoy, labeled Eyak, was deployed from a boat in the southwest corner of Elson Lagoon, near the inlet into the North Salt Lagoon (Figs. 3a,b). The water there was approximately 2 m deep (a soft mud bottom made depth difficult to measure), with a mean salinity of 19 psu

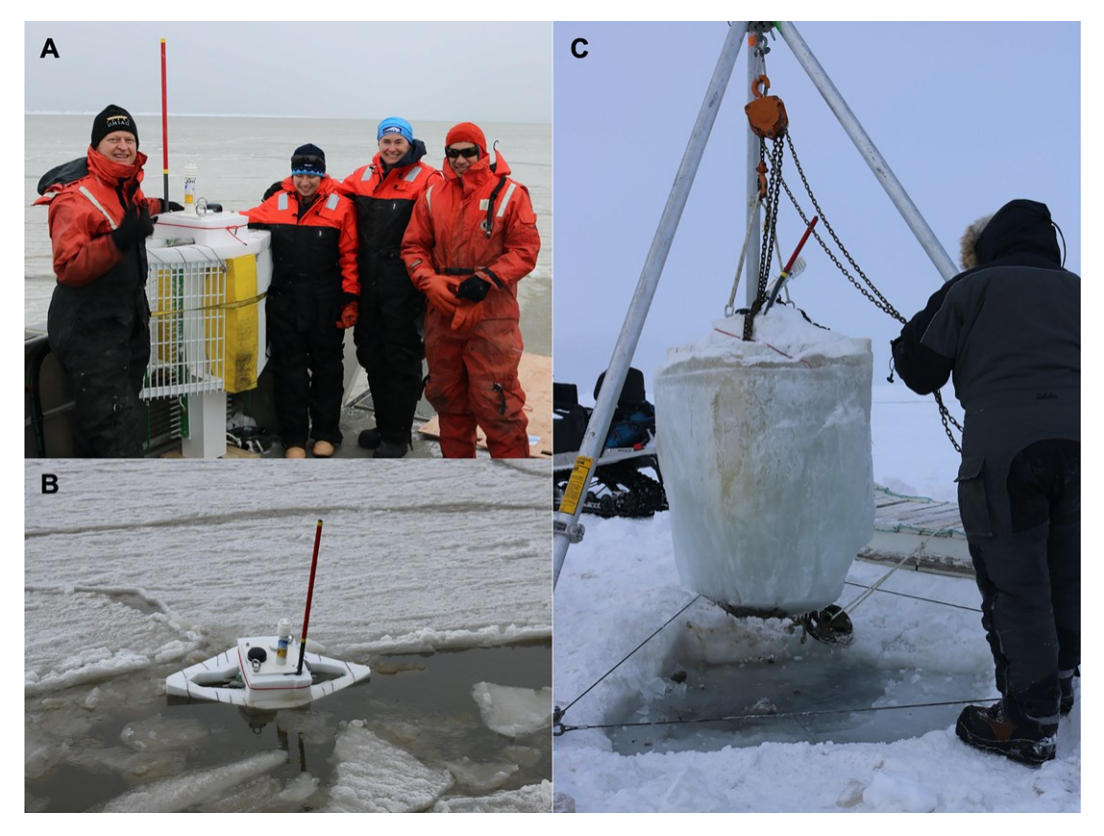


Fig. 3. Eyak MIST buoy: (a) the fully assembled buoy ready for deployment, (b) the anchored buoy just after deployment in pancake ice, and (c) the buoy being removed from the ice cover in March.

at the time of deployment (19 October 2017), there was some frazil ice floating in the water and intermittent rafts of unconsolidated slush ice approximately 5 cm thick. See Fig. 1 for local conditions.

The Eyak buoy's drag anchor held it roughly in place for the 12 h following deployment, as the slush ice built up at the surface. Unfortunately, the weather shifted and a storm came in the following day. Eyak was dragged almost a kilometer northwest until it disappeared 300 m from the spit of land bordering the west side of Elson Lagoon. It was not visible from shore the following day.

The second MIST buoy, labeled Adak, was deployed over the side of a small inflatable boat tethered to shore near the northwest corner of Elson Lagoon. It was allowed to drift, without a drag anchor, until it hit the ice edge about a kilometer away to the southeast. The buoy then stayed with the ice as the ice advanced northward, until it came to rest about 100 m from the spit bordering the north edge of the lagoon. This

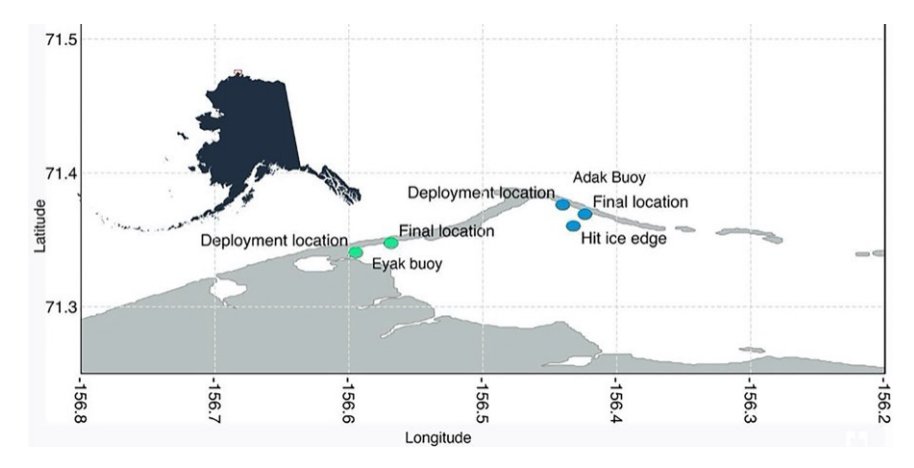


Fig. 4. Map of deployment locations in Elson Lagoon for the two buoys: Eyak and Adak.

buoy was never buried in ice and recorded data from the time of its release until the batteries died in January 2018.

In December 2017, a rescue mission armed with ice chippers and a metal detector found Eyak under a 25-cm-thick layer of ice at precisely the location of the last received GPS position. It had been run over by a floe during the storm following its deployment and spent the intervening two months under the ice, fully submerged in water. There were some scratches on the protective cage from where it had hit hard objects on the lagoon floor, two of the lowermost wire pairs on one side of the wire ladder (where they stuck out below the cage) were bent, and the air temperature post and reflective safety pole had broken. It was fully excavated from under the ice and returned to floating, where it resumed transmitting data immediately.

The two buoys continued operating through much of the winter. Adak stopped receiving data from some modules on one side in early January, and on the other side in late January, but air temperature and the remaining modules continued reporting until the buoy ran out of battery power in February. Eyak lost a few modules on one side in late February, and the battery died in early March. The batteries ran out four to five months ahead of when was expected, which we attribute to additional power drain associated with the problems with the wire ladder modules that stopped reporting data during the season.

#### e. Sea ice cores

In March of 2018, we shoveled off 10 to 20 cm of snow and cut the buoys out of the surrounding sea ice (Fig. 3c). Two cores were collected near the Eyak buoy prior to extraction in order to have a reference ice profile for further study in the laboratory. One [in hole (IH)] was from next to the buoy, and a second [out of hole (OOH)] about 8 feet away, far enough away to not have been impacted during the rescue mission. Another core was collected from the Chukchi Sea just to the west of the Eyak buoy location.

In a 2338C cold room, the OOH Eyak and Chukchi cores were cut into two vertical halves: one half for microstructural analysis and the other half for chemical analysis. Vertical thin sections were cut using a band saw, affixed to glass plates, and thinned to approximately 0.5 mm with straightedge razors. Digital images of the thin slices were recorded as JPEGs and pieced together to create full core thin sections.

The half used for analysis was then cut into 10 cm sections along the length of the core. A 2 cm slice was cut from the top of each section, cleaned by removing cut surfaces with a razor blade, and melted into a clean Nalgene bottle. Samples were also collected from the seawater beneath the sea ice at each site.

Ion chromatography was performed on the melted samples in laboratories at the Dartmouth College Earth Sciences Department and Amherst College Geology Department. Cation concentrations (Na<sup>1</sup>, Ca<sub>2</sub><sup>1</sup>, Mg<sub>2</sub><sup>1</sup>, and K<sup>1</sup>) were measured using inductively coupled plasma-optical emission spectrometry (ICP-OES). Anion concentrations (Cl<sup>2</sup> and SO<sub>4</sub><sup>22</sup>) were measured using a Dionex Ion Chromatograph.

Salinity profiles were generated by taking the sum of the concentration of major ions including sodium, magnesium, chloride, and sulfate in parts per thousand (ppt).

Oxygen isotope analysis was done to identify any freshwater input at the site, which would impact sea ice development. Delta d or the ratio of <sup>18</sup>O to <sup>16</sup>O compared to the international standard Vienna Standard Mean Ocean Water (VSMOW) is used to identify enrichment or depletion in <sup>18</sup>O (Smith et al. 2015).

Positive values of d18O indicate enrichment in 18O and depletion of <sup>16</sup>O while negative values indicate enrichment in <sup>16</sup>O and depletion of <sup>18</sup>O (Gow and Epstein 1972). Seawater presents a relatively constant d<sup>18</sup>O around the globe close to 21& or 0& (Toyota et al. 2013). Precipitation including snow, however, exhibits values ranging from 210 & to 230 & (Smith et al. 2012). While the fractionation in the atmosphere leads to large deviations between the seawater and precipitation, the fractionation during sea ice formation is small in comparison (Gow and Epstein 1972). Isotope analysis was performed in Professor Xiahong Feng's Geochemistry Stable Isotope Laboratory at Dartmouth College. The 500 µL portions of the samples were placed in small vials. The vials were then rinsed with a combination of 0.3% CO<sub>2</sub> and He for 18 h at 258C. Once the samples were equilibrated, they were placed in a Gas Chromatography Isotope Ratio Mass Spectrometer (GC-IRMS) to analyze the isotope ratios of oxygen. The GC-IRMS was connected to a Thermo Fisher Scientific GasBench to ensure accuracy and precision with a reference gas injection. The isotopic ratio of oxygen was measured and recorded by the GC-IRMS. The values were then converted to d values and uncertainties were reported within 60.1 &.

## 4. Results

The buoy outer structures survived the winter largely intact. During the overwinter deployment, the antennas did get covered by some snow but continued to operate without notable loss of signal. The air temperature sensors stayed clear of the snow, though one was broken off by something (likely a bear) late in the season. The protective cage protected the buoy from rocks and debris on the shallow lagoon floor with only minor damage (see section 3d).

Only the Eyak buoy yielded a complete vertical profile of temperature and impedance logged throughout the season. Buoy data, measured and derived, are shown in Fig. 5. Surface air temperature taken from the buoy is shown at the top (Fig. 5a) for reference. Temperature measurements (Fig. 5b) at each time and wire pair show fluctuation in response to the changing surface air temperature. As the season progressed and the ice thickened, the temperatures at depths that were in ice decreased, the result of surface air temperatures lower than water temperatures. The impedance ratio [impedance measured at a given wire pair (depth) and time divided by the impedance measured in the first two hours the buoy was in the water, Fig. 5c] increased as ice forms around the wires and highly conductive seawater is displaced by less conductive ice. The liquid fraction (Fig. 5e), the portion of the wires in water instead of ice (see section 2), decreased.

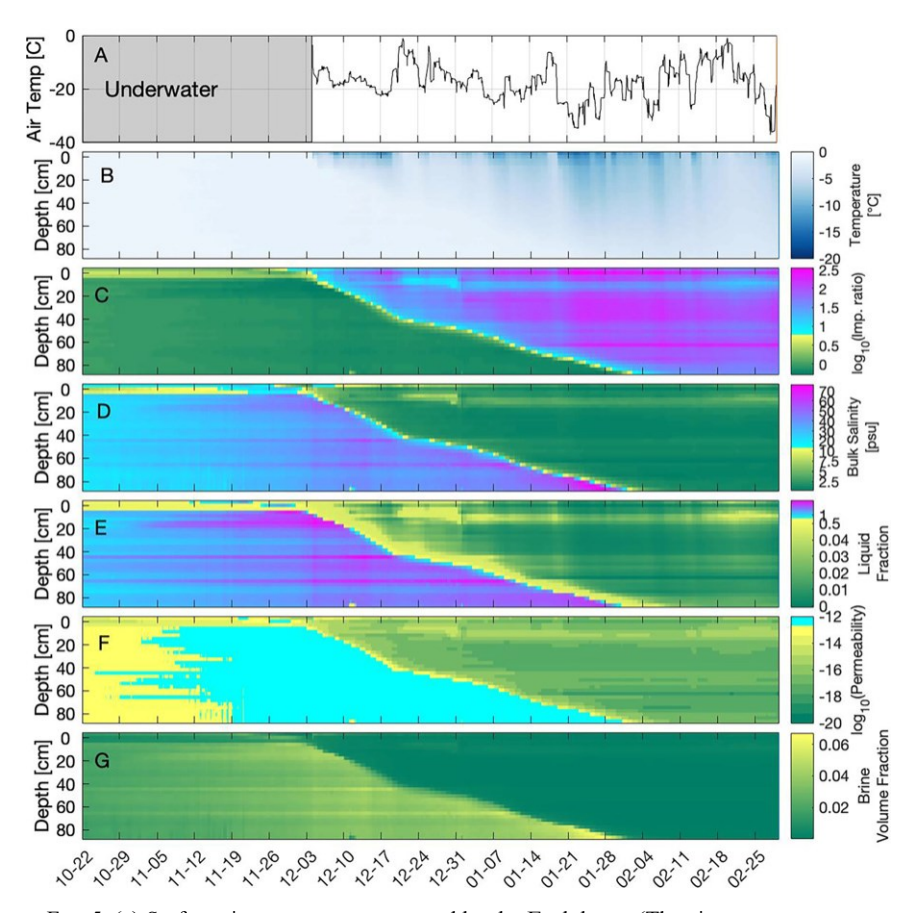


FIG. 5. (a) Surface air temperature measured by the Eyak buoy. (The air temperature sensor was underwater from late October to early December 2017.) (b),(c) Temperature and impedance ratio measured by the right-side sensor ladder on the buoy. (d)–(g) Derived products: bulk salinity, liquid fraction, permeability, and volume fraction, respectively, described in the text. Changes over the season at a given depth (e.g., 40 cm) can be seen by following progression of each data type from left to right. The figure shows the growth of the sea ice over the winter months, the influence of the temperature swings within the ice on the bulk properties, briny wa-ter left behind, and a layer about 10 cm down in the ice that maintains different properties through the latter half of the season.

The bottom four rows (Figs. 5d–g) show derived data. Bulk salinity (ice and liquid, Fig. 5d) at a given depth decreased with time as the ice fraction increased and the liquid fraction decreased. Permeability (Fig. 5f) and brine volume fraction (Fig. 5g) in the developing ice also decreased over time as the ice cover cooled and porosity decreased. By February, the entire instrument string was encased in ice, impedance was at a maximum, bulk salinity was around 2.5 psu, and brine volume fraction in the ice was at a minimum.

Figure 6 shows air temperature as measured by the Eyak buoy (red) and the Barrow Baseline Station (blue; GMD 2018). Air temperature measurements track well between the buoy and the station, about 3 km away. Some variability can be accounted for in that the air temperature sensor on the buoy was 30 cm above the designed float level (in practice, approximately 20 cm above the snow), while air temperature measurements made at the station were at the standard 2 m above ground level. Other (nontemperature) instruments at

the station on 21–23 February logged invalid data, suggesting that the anomalously high temperatures recorded on those days may not be accurate. The comparison of air temperature measured by the buoy and at the Barrow Baseline Station indicates that the warming events observed on the ice are driven by shifting weather patterns, as opposed to localized warming resulting from a small-scale lead. The station measurements were more likely to capture rapid changes in air temperature.

The ice cores were used to compare the ice at the two locations in the lagoon to nearshore ice in the open ocean. While the sea ice cover in the Chukchi Sea was 30 cm thicker (130 cm total), the top 68%–69% of each core was granular (frazil) ice, while the bottom 31%–32% was columnar.

Plots of salinity with respect to depth in sea ice cores are typically C shaped; convective overturning or gravity drainage during freezing produces relatively freshwater ice, while the highly saline component is contained in brine channels and at the advancing ice-ocean interface (Notz et al. 2005; Notz and

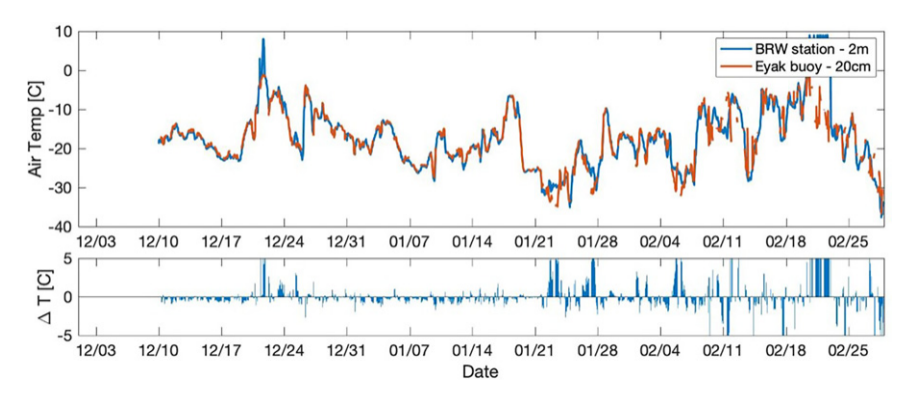


Fig. 6. (top) Surface air temperature measured by the Eyak buoy and 2 m air temperature measured at the nearby Barrow Baseline Meteorological Station, over the period of operation. (bottom) The difference in air temperature between the two measurement sites. Aside from 21 to 23 Feb, when station measurements are in question, the buoy recorded surface air temperature within a few degrees except for during periods of rapidly changing temperatures.

Worster 2008). This is exactly what was seen in both the ice core taken a short distance from the Eyak buoy and the one from the Chukchi Sea. Bulk salinity of the melted core samples was around 8 psu in the shallowest sample (5 cm), and decreased to 5 psu at 25 cm. In the Chukchi core, salinities are between 4 and 5 psu down to 115 cm and then back to 5 psu in the lowermost sample (125 cm). The salinity profile from the Elson Lagoon (Eyak) core has an almost identical shape, with the exception of 35 to 65 cm where the salinity was 3.5 psu (and 2.5 psu at 55 cm).

The range of salinities measured was quite low in both locations. At the top, it may have been lower because the ice was covered by a thick layer of snow. It was noticeable that the salinity dipped much lower in the core from Elson Lagoon (the Eyak buoy site core), to 2.5 psu instead of 4.7 psu at 55 cm depth compared to the Chukchi Sea core.

The oxygen isotope ratio (d<sup>18</sup>O) in the Chukchi core was 22.5 & at the surface but otherwise between 0 & and 1 & to the bottom of the core. The d<sup>18</sup>O values in the Eyak core were much lower in the top 80 cm: 29 & at the surface, increasing gradually to 22 & at 80 cm depth. The d<sup>18</sup>O values of the bottom two samples, at 90 and 100 cm of depth, were almost identical to those of the bottom two samples of the Chukchi core (120 and 130 cm), and the d<sup>18</sup>O of the water from the two locations was also similar (21.8 & at the Eyak site versus 21.5 & in the Chukchi).

#### 5. Discussion

# a. MIST buoy performance

The buoy exostructure was robust enough to survive the season, with the exception of the antenna structure and associated wiring. Future versions of the MIST buoy will have taller masts, and we should note that the IABP has had better success with these masts on the drift ice where wildlife is less common.

However, buoy deployment in locations prone to ice deformation, especially in marginal ice zones and coastal ice, remains

a challenge. Because the buoy with the drag anchor (Eyak) was pulled under as the ice moved, we do not recommend the drag anchor if a buoy can be allowed to drift prior to freeze up.

Omitting the drag anchor may help keep buoys from being overrun by ice floes, but the trade-off is limited control over where a buoy may end up. Near shore, this presents a particular risk of finding your buoy on the beach rather than in the water, or far from the coastline out of retrievable range.

Stresses associated with flooding in mid-January near the Adak site may have loosened the electrical connections and contributed to channel failures in several of the wire ladder modules on that buoy. A similar problem}several modules stopped recording data midseason}occurred on the Eyak buoy without any known event adding environmental stress. The exact cause of the failure is unknown but disconnecting and reconnecting the modules a couple times fixed it following the retrieval of the buoys. Replicating the issue in the laboratory has been unsuccessful, as it had only occurred after months of operation in the field.

Buoy systems carrying new sensor designs should have robust software reset options so that if there are any problems with individual channels, they need not impact the rest of the channels. Additional testing (including a long-running cold room test) is necessary to establish the reliability of the wire ladder design moving forward.

## b. Data interpretation and validation

The data show that the newly formed ice was highly sensitive to the air conditions above. Ice would cool from the top as the atmospheric temperatures dropped, but warm again quickly when atmospheric temperatures rose above the ice surface temperature.

During the first of the warming events (20–27 December), air temperatures reached as high as 21.08C (measured at the buoys and at the Barrow NOAA Baseline Observatory) (GMD 2018). Buoy data (Fig. 5) show a corresponding increase in temperature in the top 20 cm of the ice, which is correlated with a decrease in the impedance ratio between 10 and 17 cm

depth. Derived data reflect this: e.g., the marked increase in the calculated liquid fraction at 5–10 cm depth (Fig. 5). This event abruptly warmed the ice, leading to an increase in bulk salinity that persisted in the top third of the ice.

During a second warm spell (4–6 January 2018) there seemed to be some internal drainage, as this layer of higher bulk salinity moved down to lower sets of sensors (15–20 cm) where it remained for the rest of the observed season.

The drainage event did not seem to make it very far into the ice: there was no evidence of changes in the bulk salinity below 20 cm. Measurements of ice core salinity in a sample taken next to Eyak (in the refrozen hole in the ice from where it was righted) confirm a relatively high salinity layer within the ice at this depth (15–18 cm), with up to 11 psu bulk salinity in a 22 cm cube.

The major warming event later in the season (late February) seemed to make less of a difference in the ice. Liquid fraction and permeability (see Fig. 5) increased, consistent with higher temperatures allowing brine channels to open. As temperatures started to decrease again these parameters were returning to their prior state. Unfortunately, the battery on Eyak died shortly after this warming event, so the lasting consequences for the ice were not measured.

Because Elson Lagoon is shallow, brine expelled from the freezing ice does not have far to sink. Salinity measurements in Fig. 5 show increasing water salinity throughout the season, measuring up to 70 psu by the end of February. The buoy calibration procedure was not designed for salinity this high, so these numbers come with a lot of uncertainty, but local water salinity was certainly well above typical for seawater. This process decreases the local freezing point, slowing ice growth through the season.

## c. Ice growth context

The buoys in Elson Lagoon measured different ice conditions than they would have if deployed in the open ocean, in either the Chukchi or Beaufort Seas nearby. Ice in the lagoon, despite freezing up earlier, was generally thinner than ice on the ocean sides of the spit. It was also less deformed, closer to snow-covered land areas, and for most of the season grew out of higher salinity water.

Both ice cores from the Eyak buoy location and the Chukchi Sea had low d<sup>18</sup>O values in the top 10 cm, and this may suggest that the granular ice there is actually snow ice, snow that was flooded with seawater and refrozen (Smith et al. 2012). The ice at the Eyak site, however, was significantly lower in d<sup>18</sup>O than that at the Chukchi site down to a depth of 90 cm. As mentioned earlier, precipitation, including snow, has d<sup>18</sup>O values ranging from 210 & to 230 & (Smith et al. 2012). While the two locations were only about a kilometer apart, the location of the Elson Lagoon site, surrounded by land on two sides (west and south) most likely means that it receives significant blowing snow from nearby land. The Chukchi site is near only the spit of land to Point Barrow, and any blowing snow would have come over open water (there are often open leads offshore there) or sea ice.

While stable oxygen isotope fractionation in sea ice is small compared to that in the atmosphere, it has been used to determine changes in the rate of growth of sea ice in Antarctica (Toyota et al. 2013; Smith et al. 2015). It may be that the similar variations in d<sup>18</sup>O values between 50 and 80 cm in both cores could be correlated with changes in surface temperature during the season, but a full analysis of this possibility is beyond the scope of this paper.

What is interesting, however, is that the ice thickness at these nearby sites was so different, 100 cm at the Eyak buoy site and 130 cm in the Chukchi. The d18O of the water from the Elson Lagoon location was only slightly more negative than that of the water collected at the Chukchi site. This may reflect the slight influence of freshwater sources in the lagoon. However, the salinity and oxygen isotope fractionation profiles in the lower 20 cm of each core were nearly identical, suggesting that each grew unimpeded. Also, the Elson Lagoon core did not appear to have been frozen to the bottom, there was no sediment layer on the base. This core was 30 cm shorter than the one from nearby in the Chukchi Sea not because the ice is freezing to the bottom of the lagoon, but because the brine drainage slowed or stopped. Recall that water by the end of February was 70 psu. The lagoon is so shallow, and currents at the bottom in winter likely so minimal, that the brine is trapped and convectional overturning ceases. Thus, it is not merely a more protected site than the open sea on the other side of the point, nor one with significantly fresher water. It is a site whose depth limits sea ice growth.

## 6. Conclusions and recommendations

Significant effort has been expended over recent decades to develop ways to monitor sea ice extent, thickness, and mass balance. We have introduced a new way, using MIST, an instrumented buoy based on the Notz wire harp, that can help us monitor not only temperature, and hence freeze up and sea ice thickness, but also the progression of sea ice development throughout the season, e.g., the extent of cover at a given depth as it grows (solid fraction), the brine volume of the ice, and the salinity of the water just below, which is driven by brine expulsion or melting and drainage.

In initial field work, we tested two MIST buoys from the beginning of freeze up to late winter. Based on this experience, two recommendations for future improvements to the buoy can be made.

- Wire connections between sensors and between the sensors and the control system must be completely secured to withstand rough treatment and battering during the freeze-up season.
- Autonomous buoy systems should have a robust software reset option, so that if there are any problems with individual channels, they need not impact the rest of the channels.

The MIST buoy has the potential to collect detailed microstructural information over time and help us monitor all parts of the growth/melt cycle including not only the freezing process but the effects of meteorological changes, changing snow cover, the interaction of meltwater, and drainage. We believe this will be useful for understanding interannual feedback processes in sea ice, a key uncertainty in future climate projections.

One area which will need further exploration is that of the changes due to changes in freshwater influx. The Arctic receives the highest volume of terrestrial freshwater of any ocean, about 10% of the global river discharge flows into an ocean containing only 1% of the global ocean volume (Opsahl et al. 1999). Higher river inflow, the result of more increased precipitation and melting permafrost, is already having an impact on ocean temperatures and sea ice. Even leaving aside their dynamic effects (e.g., currents), freshwater sources alter the thermodynamic processes driving sea ice formation, which in turn alter its microstructure (Nakawo and Sinha 1984; Petrich et al. 2006). We anticipate using the MIST buoys to understand sea ice growth and microstructure in locations which receive significant freshwater contributions from major rivers or glacial meltwater. Further, the Arctic is experiencing more winter days above freezing than previously observed (Boisvert et al. 2016). When these events contribute to internal melt and draining in sea ice, MIST buoys could detect midwinter changes in ice structure.

All told, MIST buoys show that changes in ice properties can be measured in situ during the winter. While further development is necessary for reliable measurements throughout the season, these buoys have demonstrated that this approach can work.

Acknowledgments. This publication was prepared under NSF Grant 1935587. We thank Professor Dirk Notz of Universität Hamburg and the Max-Planck-Institut für Meteorologie for sharing his wire harps and expertise and for collaborating with us over the course of 9 years, Leif Riemenschneider of the Max-Planck-Institut für Meteorologie for building the wire harp modules we used and for his invaluable instructions and support, Professor Xiahong Feng of Dartmouth College for the use of her laboratory and her support, and Emily Martinez and Mary Margaret Stoll for their assistance with data collection and analysis. Finally, we thank two anonymous reviewers whose input contributed substantially to the quality of this paper.

Data availability statement. The data from the two buoys are openly available from the NSF Arctic Data Center at https://doi.org/10.18739/A26W9696T.

#### REFERENCES

- Bauch, D., J. A. Hölemann, A. Nikulina, C. Wegner, M. A. Janout, L. A. Timokhov, and H. Kassens, 2013: Correlation of river water and local sea-ice melting on the Laptev Sea shelf (Siberian Arctic). J. Geophys. Res. Oceans, 118, 550–561, https://doi.org/10.1002/jgrc.20076.
- Bintanja, R., and O. Andry, 2017: Towards a rain-dominated Arctic. Nat. Climate Change, 7, 263–267, https://doi.org/10.1038/nclimate3240.

- Boisvert, L. N., A. A. Petty, and J. C. Stroeve, 2016: The impact of the extreme winter 2015/16 Arctic cyclone on the Barents-Kara Seas. Mon. Wea. Rev., 144, 4279–4287, https://doi.org/10.1175/MWR-D-16-0234.1.
- Bradley, A., R. Obbard, and I. Rigor, 2020: In situ sea ice temperature and relative conductivity measurements from MIST buoy in Elson Lagoon, October 2017–March 2018. Arctic Data Center, https://doi.org/10.18739/A26W9696T.
- Carpenter, L. J., and Coauthors, 2005: Abiotic source of reactive organic halogens in the sub-Arctic atmosphere. Environ. Sci. Technol., 39, 8812–8816, https://doi.org/10.1021/es050918w.
- Centurioni, L., A. Horányi, C. Cardinali, E. Charpentier, and R. Lumpkin, 2017: A global ocean observing system for measuring sea level atmospheric pressure: Effects and impacts on numerical weather prediction. Bull. Amer. Meteor. Soc., 98, 231–238, https://doi.org/10.1175/BAMS-D-15-00080.1.
- Collins, M., and Coauthors, 2013: Long-term climate change: Projections, commitments and irreversibility. Climate Change 2013: The Physical Science Basis, T. F. Stocker et al., Eds., Cambridge University Press, 1029–1136.
- Comiso, J. C., C. L. Parkinson, R. Gersten, and L. Stock, 2008: Accelerated decline in the Arctic sea ice cover. Geophys. Res. Lett., 35, L01703, https://doi.org/10.1029/2007GL031972.
- } } , D. K. Hall, and I. Rigor, 2019: Ice surface temperatures in the Arctic region. Taking the Temperature of the Earth: Steps Towards Integrating Understanding of Variability and Change, G. C. Hulley and D. Ghent, Eds., Elsevier, 151–184.
- Cox, G. F. N., and W. F. Weeks, 1986: Changes in the salinity and porosity of sea-ice samples during shipping and storage. J. Glaciol., 32, 371-375, https://doi.org/10.1017/ S0022143000012065.
- Dimova, N. T., A. Paytan, J. D. Kessler, K. J. Sparrow, F. Garcia-Tigreros Kodovska, A. L. Lecher, J. Murray, and S. M. Tulaczyk, 2015: Current magnitude and mechanisms of groundwater discharge in the Arctic: Case study from Alaska. Environ. Sci. Technol., 49, 12036–12043, https://doi.org/10.1021/acs.est.5b02215.
- Eicken, H., 2000: From the microscopic to the macroscopic, to the regional scale: Growth, microstructure, and properties of sea ice. Sea Ice: An Introduction to its Physics, Chemistry, Biology and Geology, D. Thomas and G. S. Dieckmann, Eds., Blackwell Science, 22–81.
- GMD, 2018: Barrow Atmospheric Baseline Observatory, United States (BRW) meteorology, hourly averages, December 2017–March 2018. NOAA/ESRL, accessed 18 July 2021, https://gml.noaa.gov/dv/data/index.php?parameter\_name= Meteorology&site=BRW&frequency=Hourly%2BAverages.
- Golden, K. M., H. Eicken, A. L. Heaton, J. Miner, D. J. Pringle, and J. Zhu, 2007: Thermal evolution of permeability and microstructure in sea ice. Geophys. Res. Lett., 34, L16501, https://doi.org/10.1029/2007GL030447.
- Gow, A. J., and S. Epstein, 1972: On the use of stable isotopes to trace the origins of ice in a floating ice tongue. J. Geophys. Res., 77, 6552–6557, https://doi.org/10.1029/JC077i033p06552.
- Grenfell, T. C., 1983: A theoretical model of the optical properties of sea ice in the visible and near infrared. J. Geophys. Res., 88, 9723–9735, https://doi.org/10.1029/JC088iC14p09723.
- Harris, C. M., J. W. McClelland, T. L. Connelly, B. C. Crump, and K. H. Dunton, 2017: Salinity and temperature regimes in eastern Alaskan Beaufort Sea lagoons in relation to source water contributions. Estuaries Coasts, 40, 50–62, https://doi. org/10.1007/s12237-016-0123-z.

- IPCC, 2014: Climate Change 2013: The Physical Science Basis. Cambridge University Press, 1535 pp., https://doi.org/10.1017/ CBO9781107415324.
- Jackson, K., J. Wilkinson, T. Maksym, D. Meldrum, J. Beckers, C. Haas, and D. Mackenzie, 2013: A novel and low-cost sea ice mass balance buoy. J. Atmos. Oceanic Technol., 30, 2676–2688, https://doi.org/10.1175/JTECH-D-13-00058.1.
- Lehner, F., C. C. Raible, D. Hofer, and T. F. Stocker, 2012: The freshwater balance of polar regions in transient simulations from 1500 to 2100 AD using a comprehensive coupled climate model. Climate Dyn., 39, 347–363, https://doi.org/10. 1007/s00382-011-1199-6.
- Lieb-Lappen, R. M., E. J. Golden, and R. W. Obbard, 2017a: Metrics for interpreting the microstructure of sea ice using X-ray micro-computed tomography. Cold Reg. Res. Technol., 138, 24–37, https://doi.org/10.1016/j.coldregions.2017.03.001.
- } } , D. D. Kumar, S. D. Pauls, and R. W. Obbard, 2017b: A network model for characterizing brine channels in sea ice. Cryosphere, 12, 1013–1026, https://doi.org/10.5194/tc-12-1013-2018
- Light, B., G. A. Maykut, and T. C. Grenfell, 2003: Effects of temperature on the microstructure of first-year Arctic sea ice. J. Geophys. Res., 108, 3051, https://doi.org/10. 1029/2001JC000887.
- } } , } } , and } } , 2004: A temperature-dependent, structural-optical model of first-year sea ice. J. Geophys. Res., 109, C06013, https://doi.org/10.1029/2003JC002164.
- Nakawo, M., and N. K. Sinha, 1984: A note on brine layer spacing of first-year sea ice. Atmos.—Ocean, 22, 193–206, https://doi. org/10.1080/07055900.1984.9649193.
- Nghiem, S. V., D. K. Hall, I. G. Rigor, P. Li, and G. Neumann, 2014: Effects of Mackenzie River discharge and bathymetry on sea ice in the Beaufort Sea. Geophys. Res. Lett., 41, 873– 879, https://doi.org/10.1002/2013GL058956.
- Notz, D., and M. G. Worster, 2008: In situ measurements of the evolution of young sea ice. J. Geophys. Res., 113, C03001, https://doi.org/10.1029/2007JC004333.
- } } , J. S. Wettlaufer, and M. G. Worster, 2005: A non-destructive method for measuring the salinity and solid fraction of growing sea ice in situ. J. Glaciol., 51, 159–166, https://doi.org/10. 3189/172756505781829548.
- NSIDC, 2018: Nearing the Arctic's seasonal minimum. University of Colorado, http://nsidc.org/arcticseaicenews/2018/09/.
- Nummelin, A., M. Ilicak, C. Li, and L. H. Smedsrud, 2016: Consequences of future increased Arctic runoff on Arctic Ocean stratification, circulation, and sea ice cover. J. Geophys. Res. Oceans, 121, 617–637, https://doi.org/10.1002/2015JC011156.
- Obbard, R. W., G. Troderman, and I. Baker, 2009: Imaging brine and air inclusions in sea ice using micro X-ray computed tomography. J. Glaciol., 55, 1113–1115, https://doi.org/10.3189/002214309790794814.

- } } , R. Lieb-Lappen, K. V. Nordick, E. J. Golden, J. R. Leonard, A. Lanzirotti, and M. G. Newville, 2016: Synchrotron X-ray fluorescence spectroscopy of salts in natural sea ice. Earth Space Sci., 3, 463–479, https://doi.org/10.1002/2016EA000172.
- Opsahl, S., R. Benner, and R. M. W. Amon, 1999: Major flux of terrigenous dissolved organic matter through the Arctic Ocean. Limnol. Oceanogr., 44, 2017–2023, https://doi.org/10.4319/lo.1999.44.8.2017.
- Parkinson, C. L., and J. C. Comiso, 2013: On the 2012 record low Arctic sea ice cover: Combined impact of preconditioning and an August storm. Geophys. Res. Lett., 40, 1356–1361, https://doi.org/10.1002/grl.50349.
- Petrich, C., P. J. Langhorne, and Z. F. Sun, 2006: Modelling the interrelationships between permeability, effective porosity and total porosity in sea ice. Cold Reg. Sci. Technol., 44, 131– 144, https://doi.org/10.1016/j.coldregions.2005.10.001.
- Smith, I. J., A. J. Gough, P. J. Langhorne, A. R. Mahoney, G. H. Leonard, R. Van Hale, and T. G. Haskell, 2015: First-year land-fast Antarctic sea ice as an archive of ice shelf meltwater fluxes. Cold Reg. Sci. Technol., 113, 63–70, https://doi.org/10.1016/j.coldregions.2015.01.007.
- Smith, T. M., P. A. Arkin, L. Ren, and S. S. P. Shen, 2012: Improved reconstruction of global precipitation since 1900.
  J. Atmos. Oceanic Technol., 29, 1505–1517, https://doi.org/10.1175/JTECH-D-12-00001.1.
- Steele, M., A. C. Bliss, G. Peng, W. N. Meier, and S. Dickinson, 2019: Arctic sea ice seasonal change and melt/freeze climate indicators from satellite data, version 1. NASA National Snow and Ice Data Center Distributed Active Archive Center, accessed 1 November 2020, https://doi. org/10.5067/KINANQKEZI4T.
- Stroeve, J. C., T. Markus, L. Boisvert, J. Miller, and A. Barrett, 2014: Changes in Arctic melt season and implications for sea ice loss. Geophys. Res. Lett., 41, 1216–1225, https://doi.org/10. 1002/2013GL058951.
- Strong, C., and I. G. Rigor, 2013: Arctic marginal ice zone trending wider in summer and narrower in winter. Geophys. Res. Lett., 40, 4864–4868, https://doi.org/10.1002/grl.50928.
- Toyota, T., I. J. Smith, A. J. Gough, P. J. Langhorne, G. H. Leonard, R. J. Van Hale, and T. G. Haskell, 2013: Oxygen isotope fractionation during the freezing of sea water. J. Glaciol., 59, 697– 710, https://doi.org/10.3189/2013JoG12J163.
- Vancoppenolle, M., G. Madec, M. Thomas, and T. J. McDougall, 2019: Thermodynamics of sea ice phase composition revisited. J. Geophys. Res. Oceans, 124, 615–634, https://doi.org/10. 1029/2018JC014611.
- Worster, M. G., and D. W. Rees Jones, 2015: Sea-ice thermodynamics and brine drainage. Philos. Trans. Roy. Soc., A373, 20140166, https://doi.org/10.1098/rsta.2014.0166.